

University of Massachusetts Medical School
eScholarship@UMMS

UMass Metabolic Network Publications

UMass Metabolic Network

2017-06-13


MAP4K4 impairs energy metabolism in endothelial cells and promotes insulin resistance in obesity

Rachel J. Roth Flach
University of Massachusetts Medical School

Et al.

Let us know how access to this document benefits you.

Follow this and additional works at: https://escholarship.umassmed.edu/metnet_pubs

 Part of the [Biochemistry Commons](#), [Cell Biology Commons](#), [Cellular and Molecular Physiology Commons](#), and the [Molecular Biology Commons](#)

Repository Citation

Roth Flach RJ, DiStefano MT, Danai LV, Senol-Cosar O, Yawe JC, Kelly M, Garcia Menendez L, Czech MP. (2017). MAP4K4 impairs energy metabolism in endothelial cells and promotes insulin resistance in obesity. UMass Metabolic Network Publications. <https://doi.org/10.1152/ajpendo.00037.2017>. Retrieved from https://escholarship.umassmed.edu/metnet_pubs/102

This material is brought to you by eScholarship@UMMS. It has been accepted for inclusion in UMass Metabolic Network Publications by an authorized administrator of eScholarship@UMMS. For more information, please contact Lisa.Palmer@umassmed.edu.

1
2
3
4
5
6
7
8
9
10
11
12
13
14
15
16
17
18
19
20
21
22
23
24
25
26
27
28
29
30
31
32
33
34
35
36
37
38
39
40
41
42
43

MAP4K4 impairs energy metabolism in endothelial cells and promotes insulin resistance in obesity

Rachel J. Roth Flach^{1*}, Marina T. DiStefano², Laura V. Danai³, Ozlem Senol-Cosar², Joseph C. Yawe⁴, Mark Kelly⁵, Lorena Garcia Menendez, Michael P. Czech

Program in Molecular Medicine,
University of Massachusetts Medical School, Worcester, MA 01605, USA

Author contributions: R.J.R.F. and M.P.C designed research, R.J.R.F., L.V.D., L.G.M., M.T.D., O. S-C., J.C.Y. and M.K. performed research, and R.J.R.F and M.P.C wrote the manuscript.

Running title: Endothelial MAP4K4 in metabolism

Key words: Endothelial, MAP4K4, obesity, lymphatic, inflammation

Classification: Biological Sciences; Medical Sciences

***Address correspondence to:**

Rachel J. Roth Flach
Pfizer, Inc.
1 Portland St, 307J
Cambridge, MA 02139
e-mail: Rachel.Rothflach@pfizer.com

44 **Abstract**

45 The blood vasculature responds to insulin, influencing hemodynamic
46 changes in the periphery, which promotes tissue nutrient and oxygen delivery
47 and thus metabolic function. The lymphatic vasculature regulates fluid and lipid
48 homeostasis, and impaired lymphatic function can contribute to atherosclerosis
49 and obesity. Recent studies have suggested a role for endothelial cell (EC)
50 Mitogen activated protein kinase kinase kinase kinase 4 (Map4k4) in
51 developmental angiogenesis and lymphangiogenesis as well as atherosclerosis.
52 Here, we show that inducible EC Map4k4 deletion in adult mice ameliorates
53 metabolic dysfunction in obesity despite the development of chylous ascites and
54 a concomitant striking increase in adipose tissue lymphocyte content. Despite
55 these defects, animals lacking endothelial Map4k4 were protected from skeletal
56 muscle microvascular rarefaction in obesity, and primary ECs lacking Map4k4
57 displayed reduced senescence and increased metabolic capacity. Thus,
58 endothelial Map4k4 has complex and opposing functions in the blood and
59 lymphatic endothelium post-development. Whereas blood endothelial Map4k4
60 promotes vascular dysfunction and impairs glucose homeostasis in adult
61 animals, lymphatic endothelial Map4k4 is required to maintain lymphatic vascular
62 integrity and regulate immune cell trafficking in obesity.

63

64

65

66

67 **Introduction**

68 Type 2 diabetes (T2D) is associated with impaired glucose homeostasis, insulin
69 resistance and an increased inflammatory state (16, 35, 43, 46). Though much work has
70 sought to investigate the mechanisms by which T2D occurs and how to ameliorate this
71 disease, there is still a lack of mechanistic understanding of the contribution of individual
72 physiological systems to disease progression. In particular, the vascular endothelium
73 has been investigated as a contributor to T2D pathology (18, 19, 41). Endothelial cells
74 line the blood and lymphatic vasculature within every tissue, and the vascular
75 endothelium has a unique role to communicate nutritional and inflammatory status of
76 underlying tissue to the systemic circulation by delivering nutrients, hormones and
77 oxygen (1). Conversely, the lymphatic endothelium regulates fluid balance, intestinal
78 lipid absorption, and immune function (7, 25). Recent human and mouse genetic studies
79 have suggested that the endothelium plays a multifaceted role in whole body
80 metabolism (4, 18, 19, 34, 37).

81 In obesity the endothelium becomes resistant to the hormone insulin, which
82 impairs blood flow and thus insulin and nutrient transport to tissues such as skeletal
83 muscle resulting in increased plasma glucose levels and type 2 diabetes (19, 47).
84 Furthermore, lymphatic vessels within adipose tissue can become leaky and further
85 exacerbate obesity by promoting adipogenesis (17, 32). Finally, type 2 diabetes is also
86 associated with low-grade inflammation in multiple tissues including adipose tissue and
87 liver (16), which is mediated in part by immune cell recruitment from the peripheral
88 vasculature (22, 23, 29, 30). Thus, identifying molecular targets within the vasculature
89 that mediate these dysfunctions are important for improving human health.

90 Our laboratory recently demonstrated that inducible, systemic loss of the protein
91 kinase Mitogen activated protein kinase kinase kinase 4 (Map4k4) in adult obese
92 mice improved insulin sensitivity and regulated insulin secretion (8, 26). Using
93 constitutive endothelial-specific knockout animals, we demonstrated that Map4k4 has a
94 profound and complex role to control lymphatic vascular development (27); however,
95 inducible endothelial Map4k4 deletion was beneficial in *ApoE*^{-/-} mice, as *ApoE*^{-/-} mice
96 lacking Map4k4 (28) demonstrated reduced atherosclerotic plaque development and
97 reduced leukocyte recruitment. We thus hypothesized that obese C57BL6/J mice
98 lacking endothelial Map4k4 might also display reduced obesity-induced adipose tissue
99 inflammation and therefore improved insulin sensitivity.

100 The present studies were designed to bypass the developmental phenotype
101 recently reported in constitutively expressed Cdh5 cre (Ve-Cadherin cre) Map4k4
102 endothelial-specific knockout mice (27) by generating inducible endothelial-specific
103 Map4k4 deletion in adult C57BL6/J mice using the tamoxifen-induced Cdh5(PAC)ERT2-
104 cre (44). Interestingly, chow-fed animals displayed no overt phenotype; however, when
105 challenged with a high fat diet (HFD), inducible endothelial-specific Map4k4 knockout
106 mice (M4K4 iECKO) displayed a non-significant trend to improved glucose tolerance
107 and significantly enhanced insulin sensitivity compared with controls. Despite this
108 metabolic improvement in M4K4 iECKO mice, these animals also displayed lymphatic
109 defects as noted by chyle leakage in the abdomen (chylous ascites) and increased
110 immune cell content in epididymal adipose tissue. Despite these lymphatic defects,
111 skeletal muscle capillary density was maintained after HFD in M4K4 iECKO mice
112 compared with controls, and isolated endothelial cells derived from these animals

113 displayed enhanced energy metabolism and protection from senescence. Taken
114 together, these results demonstrate a complex and critical role for endothelial Map4k4
115 to maintain lymphatic vascular integrity yet promote systemic insulin resistance in
116 obesity.

117

118 **Materials and Methods**

119

120 **Mouse models:** The University of Massachusetts Medical School Institutional Animal
121 Care and Use Committee approved all of the animal procedures. Map4k4 Flox/Flox
122 animals and M4K4 iECKO mice (Cdh5(PAC)-CreERT2) were maintained on a pure
123 C57Bl6/J background after at least 8 backcrosses and have been previously described
124 (28). At 6-8 weeks of age, male Flox/Flox and Flox/Flox/cre+ littermates were injected
125 with 1 mg tamoxifen/day in corn oil (Sigma) for 5 days; 2 weeks after tamoxifen
126 injection, the mice were fed standard chow or high fat diet (60% fat, Research diets
127 RD12492i) for 16 weeks. Mice were euthanized by CO₂ inhalation followed by bilateral
128 pneumothorax. Mice were fasted for 16 h for GTTs or for 4 h for ITTs. Fasted mice were
129 i.p. injected with glucose (1 g/kg) or insulin (1 IU/kg). Blood glucose levels were
130 determined from the tail vein using a Breeze-2 glucose meter (Bayer). No statistical
131 methods were used to predict sample size, no randomization was performed, and the
132 investigations were not blinded.

133

134 **Miles assay:** 4 weeks after tamoxifen injections, mice were injected intravenously (i.v.)
135 with 1.5% Evans Blue Dye (50 mg/kg) into the tail vein. 30 mins post-injection, mice

136 were sacrificed by cervical dislocation and perfused with saline for 10 minutes. Pieces
137 of inguinal white adipose tissue (WAT), epididymal WAT, lung and liver were excised,
138 weighed and incubated in formamide overnight at 55°C with shaking to extract the dye.
139 Absorbance of the extravasated dye was quantified by spectrophotometry at 620 nm
140 and normalized to tissue weight.

141

142 **RNA isolation and quantitative RT-PCR:** Total RNA was isolated, cDNA was
143 prepared, and quantitative RT-PCR was performed as previously described (28).
144 Primer sequences are detailed in **Table 1**.

145

146 **Immunostaining:** Whole mount staining was performed on tissues that had been fixed
147 in 10% formalin for 2-6 hours. Adipose tissue, skeletal muscle or aortic rings were
148 blocked overnight in 10% BSA and 0.3% triton X-100 in PBS at 4C, stained overnight
149 with Isolectin B4 (Life Technologies I21411; 1:40) in 100 mM MgCl₂, 100 mM CaCl₂, 10
150 mM MnCl₂, and 1% Triton X-100 in PBS at 4C, and washed 3x 20 minutes in 5% BSA,
151 0.15% triton X-100 in PBS at room temperature. Tissues were mounted in ProLong
152 Gold (Life Technologies). Whole mount images were visualized in flattened 25 um z-
153 stacks with a Solamere Technology Group modified Yokogawa CSU10 spinning disk
154 confocal system with a Nikon TE-2000E2 inverted microscope at 10x or 20x. Images
155 were acquired with MetaMorph Software, version 6.1 (Universal Imaging, Downingtown,
156 PA). A Zeiss Axiovert 100 inverted microscope with a 5x or 10x objective and AxioCam
157 HRm camera was used for aortic ring assay images. At least 3 muscle or adipose tissue
158 images were quantified and averaged for average vascular density per mouse. Images

159 were quantified using Image J Analysis Software. Different mice were used for the
160 analyses of different tissues.

161

162 **Senescence Assays:** Primary mouse lung endothelial cells (MLECs) were prepared
163 by digestion and immune-isolation using CD31 and ICAM-2-coated magnetic beads as
164 previously described (28). MLECs were used on passage 3 for all experiments.
165 Senescence was assessed in MLECs that had grown to confluence with the beta
166 galactosidase senescence assay kit (Cell Signaling) according to manufacturer's
167 instructions. Percent positive staining was determined in at least 3 5x fields using image
168 J software. Nuclei were stained with Hoechst (Sigma), and the entire well was imaged
169 using the In Cell high content imager and counted using Columbus Image data analysis
170 software. Percent positive area was normalized to nuclei number.

171

172 **Flow Cytometry:** The epididymal adipose tissue stromal vascular fraction (SVF) was
173 isolated by digestion in Hanks balanced salt solution, 2.5% BSA and 2 mg/mL
174 collagenase for 45 minutes and strained through a 70 µm filter followed by red blood cell
175 lysis (155 mM NH₄Cl, 12 mM NaHCO₃, 0.1 mM EDTA). Cells were blocked with mouse
176 IgG in FACS buffer (1% BSA/PBS). Cells were stained with antibodies directed towards
177 F4/80 (APC, ABd serotec), CD11b (Percp 5.5, BD), Siglec F (PE, BD), GR-1 (APC-Cy7,
178 BD), Ly6c (PE-Cy7, BD), Galectin 3 (FITC, BioLegend), and CD11c (V450, BD) or CD3
179 (PE-Cy7 or APC-Cy7, BD), CD4 (FITC, BD), CD8 (Percp, BD), CD25 (APC-Cy7, BD),
180 Foxp3 (PE, BD), CD19 (V450, BD), or NK1.1 (APC, BD). Foxp3 staining was performed
181 using the Foxp3/Transcription Factor Staining Buffer Set (eBioscience) according to

182 manufacturer's instructions. All antibodies were used at a 1:200 dilution. The data were
183 collected on an LSRII (BD) and were analyzed with FlowJo software. Samples were
184 gated for scatter and single cells. Lymphocyte populations were gated first on low size
185 and scatter prior to gating for positive staining. Gates were drawn based on
186 fluorescence minus one (FMO) controls. A total of at least 100,000 events were
187 recorded.

188

189 **Cellular metabolism measurements:** Confluent cell monolayers were obtained by
190 seeding 60,000 MLECs overnight on 0.2% gelatin-coated Seahorse XF24 tissue culture
191 plates (Seahorse Biosciences). Seahorse glycostress or mitostress tests were
192 performed using the standard protocol according to manufacturer's instructions on an
193 XF24 Seahorse extracellular flux analyzer. Drug concentrations were as follows:
194 Glucose (10 mM), Oligomycin (2.5 uM), 2-DG (50 mM), FCCP (1 uM), Antimycin A and
195 Rotenone (0.87 uM). Oxygen consumption rate (OCR) or extracellular acidification rate
196 (ECAR) values were normalized to protein content as assessed by BCA assay
197 (Thermo-Pierce). Each OCR or ECAR value represents an average from duplicate
198 wells.

199

200 **Statistical Analysis:** A two-tailed Student's t-test was used to compare two groups in
201 GraphPad Prism 6.0 or 7.0. Where indicated, experiments comparing multiple groups
202 were analyzed with two-way ANOVA with repeated measures. $P < 0.05$ was considered
203 to be statistically significant, and $P = 0.05-0.09$ was considered to be a non-significant
204 trend. Variance was estimated using the standard error of the mean.

205

206 **Results**

207 **Inducible EC Map4k4 loss in adult obese mice improves glucose tolerance.**

208 To bypass the lethal effects of Map4k4 deletion in development, Map4k4 was deleted
209 inducibly with tamoxifen in adult C57Bl6/J mice between 6-8 weeks of age (M4K4
210 iECKO; Fig. 1A). The deletion pattern of these mice using this protocol has been
211 previously reported and is nearly 100% after 18 weeks as assessed in primary mouse
212 lung ECs (MLECs) (28). Inducible Map4k4 deletion in these mice on a chow diet
213 revealed no obvious phenotypes, and no change in body weight was observed between
214 genotypes (Fig. 1B). Both Flox/Flox and M4K4 iECKO animals gained weight to a
215 similar extent on HFD, and no alteration in body weight or tissue weights was observed
216 and weights of all tissues including subcutaneous adipose tissue (SAT), epididymal
217 white adipose tissue (eWAT), liver and spleen were unchanged between HFD-fed
218 control and M4K4 iECKO mice (Fig. 1B-F).

219 Glucose tolerance and insulin sensitivity were next assessed in chow- and HFD-
220 fed Flox/Flox and M4K4 iECKO mice. In chow-fed Flox/Flox and M4K4 iECKO animals,
221 no alterations were observed in glucose tolerance or insulin sensitivity (Fig. 1G-H).
222 However, after HFD, Map4k4 iECKO animals demonstrated a non-significant trend to
223 improved glucose tolerance compared with Flox/Flox controls (Fig. 1G) and a significant
224 improvement in HFD-induced insulin resistance (Fig. 1H). We have previously reported
225 that mice inducibly lacking whole body Map4k4 had dramatic reductions in insulin levels
226 after HFD, which contributed to improvements in insulin sensitivity (26). Interestingly, a
227 non-significant trend to reduced insulin levels was also observed in M4K4 iECKO mice

228 after HFD compared with Flox/Flox controls (Table 2), suggesting that these animals
229 are in fact less insulin resistant than control littermates. Taken together, these data
230 suggest that M4K4 iECKO mice on HFD demonstrate enhanced insulin sensitivity
231 compared with control Flox/Flox littermates.

232 **Reduced expression of inflammation genes in liver of HFD-fed M4K4 iECKO**
233 **mice.** The intriguing improvement in insulin sensitivity in M4K4 iECKO mice suggested
234 that M4K4 expression within the vasculature was detrimental to metabolic homeostasis.
235 We had previously demonstrated that endothelial Map4k4 promoted vascular
236 inflammation in atherosclerosis by promoting leukocyte recruitment (28). Thus, we
237 hypothesized that similar mechanisms may be at play in obesity, and assessed whether
238 loss of endothelial Map4k4 ameliorated HFD-induced inflammation.

239 Histological assessment of liver from Flox/Flox and M4K4 iECKO mice revealed
240 no remarkable differences between genotypes after HFD (Fig. 2A). However, reduced
241 mRNA expression of adhesion molecule *Icam-1* was observed, and there was a non-
242 significant trend to reductions in levels of adhesion molecules *Vcam-1*, and *Selp* as well
243 as immune cell marker *F4/80* in whole liver of HFD-fed iECKO mice compared with
244 controls (Fig. 2B,C), which is consistent with previous observations that endothelial
245 Map4k4 promotes immune cell recruitment and inflammation (28).

246 **HFD-induced chylous ascites and eWAT immune cell content in M4K4**
247 **iECKO mice.** Visual inspection, flow cytometry assessment and histological
248 assessment of eWAT from chow-fed control and M4K4 iECKO mice did not reveal any
249 significant changes in appearance or immune cell content (Figure 3 and not shown).
250 However, chylous ascites was observed in approximately 50% of HFD-fed M4K4 iECKO

251 mice (Fig. 3A). In addition, the HFD-fed M4K4 iECKO mice displayed a striking increase
252 in adipose tissue immune cell infiltration in eWAT after HFD, even in animals where no
253 noticeable chyle leakage was present (Fig. 3B). This observation was surprising
254 because increased eWAT inflammation in obesity is associated with glucose intolerance
255 and insulin resistance in humans and in mice (16), and M4K4 iECKO mice displayed
256 enhanced insulin sensitivity on HFD (Fig. 1G-H). This phenotype seemed to be confined
257 to eWAT, as retroperitoneal white adipose tissue (rWAT), mesenteric WAT (mWAT),
258 subcutaneous WAT (SAT), and intrascapular brown adipose tissue (BAT) histology
259 revealed no significant alterations in tissue morphology between the genotypes after
260 HFD (Fig. 3C).

261 Numerous studies have demonstrated that macrophages are the predominant
262 immune cell type in obese AT and accumulate in crown-like structures that surround
263 adipocytes (45, 48). However, the inflammatory phenotype observed within the M4K4
264 iECKO eWAT was not characteristic of crown-like structures and instead resembled
265 dense cell clusters with small, dark nuclei (Fig. 3B). This observation coupled with the
266 chyle leakage observed in M4K4 iECKO mice (Fig. 3A) suggested that this cell
267 population might be atypical. To elucidate what cell types comprised the immune cells
268 within the adipose tissue, the stromal vascular fraction (SVF) was isolated from eWAT,
269 and flow cytometry was performed. Interestingly, no significant differences in the SVF
270 CD11b⁺/F4/80⁺ macrophage populations were observed between Flox/Flox and M4K4
271 iECKO mice, nor were there differences in the CD11b⁺/F4/80⁺/Cd11c⁺ pro-
272 inflammatory macrophage population (Fig. 4A, C). Furthermore, mRNA expression of
273 macrophage markers *F4/80*, *Itgam*, *Itgax* and *Cd68* and macrophage-derived cytokines

274 *Ccl-2*, *Il-1 β* , *Il-6*, and *Tnf- α* were not altered in control and iECKO HFD-fed mice (Fig.
275 4D).

276 Lymphocyte populations were then assessed within eWAT of Flox/Flox and
277 M4K4 iECKO mice. Flow cytometry of eWAT-derived SVF revealed a significant
278 increase in lymphocyte populations, as a 72% increase in Cd19⁺ B lymphocytes (3%
279 vs. 5.1% of SVF for Flox/Flox or M4K4 iECKO mice, respectively, Fig. 4E) and a 47%
280 increase in total Cd3⁺ T lymphocyte content (12.5 vs. 18.4% of SVF for Flox/Flox or
281 M4K4 iECKO mice, respectively, Fig. 4E) was observed in M4K4 iECKO mice. Further
282 assessment of T lymphocyte subsets within SVF revealed that pro-inflammatory Cd8⁺
283 as well as anti-inflammatory Cd4⁺ and Treg (Cd25⁺/Foxp3⁺) lymphocyte populations
284 were significantly enhanced in M4K4 iECKO SVF by a similar extent (Fig. 4B, E).
285 Analysis by qRT-PCR of whole eWAT also demonstrated a significant enhancement of
286 T lymphocyte markers *Cd4* and *Cd8* and a non-significant trend to an increase in *Foxp3*
287 gene expression (p=0.09) in M4K4 iECKO eWAT after HFD, but interestingly there was
288 no concomitant increase in T-cell derived cytokines *Il-4*, *Il-10*, *Ifn- γ* , *Il-13*, *Il-17*, or *IL-21*
289 (Fig. 4F). These data suggest that the lymphocyte accumulation in M4K4 iECKO eWAT
290 after HFD may be a passive accumulation of naïve lymphocytes a consequence of
291 chyle leakage into the abdominal cavity. These data also suggest that although chyle
292 leakage is only visually present in 50% of animals, there is likely lymphatic leakage and
293 dysfunction in all of the M4K4 iECKO animals, even if no chyle is observed by eye.

294 **Maintained blood vascular integrity and reduced microvascular rarefaction**
295 **in skeletal muscle of M4K4 iECKO mice.** Lymphatic dysfunction promotes obesity
296 and is associated with metabolic disease in mice (17, 32). Thus, it is intriguing that

297 despite their lymphatic chyle leakage defects, M4K4 iECKO mice are glucose tolerant
298 and insulin sensitive compared with controls. However, the VE Cadherin promoter used
299 to generate M4K4 iECKO mice deletes genes in both blood and lymphatic endothelial
300 compartments (36). Thus, we cannot exclude the possibility that the improved
301 metabolism in the M4K4 iECKO mice is due to changes in blood vascular ECs. Previous
302 studies using cell culture models demonstrated that Map4k4 loss reduces endothelial
303 cell barrier function (24, 28). Thus, vascular permeability was assessed in vivo by
304 injecting Evan's blue dye i.v. into chow fed Flox/Flox and Map4k4 iECKO mice, and no
305 differences were observed in the amount of dye that had leaked into adipose tissue,
306 liver or lung between genotypes (Fig. 5A-D). Thus, Map4k4 may not be critical to
307 maintain baseline vascular permeability in healthy mice. Angiogenesis and blood
308 vascular function is critical for metabolic homeostasis, as humans and animals with
309 angiogenic defects display metabolic dysfunction, and angiogenesis is critical to proper
310 adipose tissue expansion and health (5, 6, 14, 15, 38). To assess angiogenic potential,
311 aortic ring angiogenesis assays were performed; however, no difference was observed
312 in the number of isolectin B4-stained sprouts from Flox/Flox and M4K4 iECKO aortas
313 (Fig. 5E-F).

314 Capillary density was next assessed in tissues of the HFD-fed Flox/Flox and
315 M4K4 iECKO mice. eWAT was isolated, and whole-mount samples were
316 immunostained with isolectin B4 as a measure of capillary density. However, only a
317 non-significant trend in isolectin B4 staining was observed in HFD-fed M4K4 iECKO
318 mice (Fig. 5G-H). In skeletal muscle, capillary density is paramount for insulin-mediated
319 hemodynamic changes and reflects insulin sensitivity, and a loss of capillary density, or

320 capillary rarefaction, occurs in obesity (4, 13). To assess this, soleus muscle was
321 isolated from chow and HFD-fed Flox/Flox and M4K4 iECKO mice and stained whole-
322 mount with isolectin B4. In chow-fed mice, there was no difference in microvascular
323 density between genotypes (Fig. 5I-J). However, HFD-fed M4K4 iECKO animals were
324 resistant to capillary rarefaction compared with controls (Fig. 5I-J). These observations
325 are reminiscent to what has been previously reported in the retina using the constitutive
326 *Cdh5* promoter (27). This protection from capillary rarefaction could explain why M4K4
327 iECKO mice are insulin sensitive, as capillary rarefaction is associated with insulin
328 resistance and metabolic disease (4, 34).

329 Because loss of endothelial *Map4k4* promoted enhanced lymphatic vascular and
330 blood vascular density phenotypes in development and protected against capillary
331 rarefaction in HFD (Fig. 5) (27), we hypothesized that *Map4k4* may affect EC growth.
332 Indeed, our previous reports describe that ECs derived from M4K4 iECKO mice
333 displayed enhanced proliferation, which is relevant in development, tissue expansion,
334 and response to injury (27). In normal, uninjured tissues, microvascular ECs are mostly
335 quiescent; however, they are subject to senescence in obese states and with aging
336 (42). To assess whether replicative senescence was altered by loss of *Map4k4*, primary
337 MLECs were isolated from chow-fed Flox/Flox or M4K4 iECKO mice that had been
338 injected with tamoxifen as demonstrated in Fig. 1A. ECs senesce rapidly in culture (11);
339 thus, endogenous β -galactosidase (β -gal) activity was assessed at passage 3 in
340 confluent MLECs. Whereas Flox/Flox MLECs demonstrated abundant β -gal staining
341 consistent with senescence, M4K4 iECKO MLECs displayed a 55% reduction in

342 endogenous β -gal activity as assessed by stained area and normalized to total number
343 of nuclei (Fig. 6 A-B).

344 **Enhanced mitochondrial and glucose metabolism in ECs Lacking Map4k4.**

345 Recent studies have demonstrated that glycolysis and fatty acid oxidation are critical for
346 EC proliferation (10, 33). The reduced senescence observed in M4K4 iECKO MLECs
347 (Fig. 6A-B) suggested that these cells might be more metabolically active than Flox/Flox
348 controls (49). Our laboratory originally identified Map4k4 as a negative regulator of
349 glucose uptake in adipocytes (40); thus, ECs lacking Map4k4 may also display
350 increased glycolysis and metabolic flux. Mitochondrial and glycolytic function was
351 assessed in Flox/Flox and M4K4 iECKO MLECs using the Seahorse extracellular flux
352 analyzer. In a mitochondrial stress test, the basal oxygen consumption rate (OCR) and
353 mitochondrial coupling efficiency were similar between genotypes (Fig. 6C-D). However,
354 when the mitochondria were uncoupled with Carbonyl cyanide-4-
355 (trifluoromethoxy)phenylhydrazone (FCCP), a dramatic increase in oxygen consumption
356 was observed indicating increased spare capacity of the mitochondria in M4K4 iECKO
357 MLECs compared with Flox/Flox controls (Fig. 6C-D). When subjected to a glycolysis
358 stress test, no changes in acidification rates in response to glucose alone were
359 observed, suggesting that basal glycolysis was similar between genotypes (Fig. 6E-F).
360 However, when M4K4 iECKO MLECs were treated with oligomycin to inhibit
361 mitochondrial ATP production, the increased acidification rate demonstrated a non-
362 significant trend to enhanced glycolytic capacity, as well as a significant increase in
363 glycolytic reserve (Fig. 6E-F). These data suggest that loss of Map4k4 in ECs allows for
364 a better response to energy stress and could therefore contribute to the improved

365 metabolic phenotype and the protection from capillary rarefaction that was observed in
366 M4K4 iECKO mice despite lymphatic abnormalities.

367

368 **Discussion**

369 These studies reveal a complex role of endothelial protein kinase Map4k4 to
370 promote whole-body metabolic dysfunction. Using tamoxifen-inducible
371 Cdh5(PAC)ERT2-cre to delete endothelial Map4k4 in adult C57Bl6/J mice, we observed
372 that loss of endothelial Map4k4 improved insulin sensitivity in obesity (Fig. 1). Mice
373 lacking endothelial Map4k4 displayed unaltered adipose tissue size or hepatic lipid
374 content but reduced inflammatory gene expression in liver (Fig. 2). Loss of endothelial
375 Map4k4 also caused chyle leakage and immune cell infiltration in eWAT (Figs. 3-4),
376 presumably due to lymphatic vascular deficiencies. These phenotypes seem to
377 counteract each other; while Map4k4 expression is detrimental in the blood vasculature,
378 it is required for normal lymphatic vascular function. These observations are consistent
379 with previous observations in development, in which loss of endothelial Map4k4 through
380 use of constitutively expressed Ve Cadherin-Cre led to postnatal lethality due to fluid
381 leakage and chylothorax (27). These observations are also consistent with our previous
382 study in *ApoE*^{-/-} mice, in which mice lacking endothelial Map4k4 were protected from
383 atherosclerosis development (28). Chyle leakage was not observed in *ApoE*^{-/-} mice
384 lacking endothelial Map4k4 after deletion with tamoxifen using the same cre driver
385 (Cdh5(PAC) Ve-ERT2) and injection protocol described here; however, the lymphatics
386 in *ApoE*^{-/-} mice are dysfunctional, which could account for this difference (20, 21, 39).

387 Though apparent lymphatic defects were observed in M4K4 iECKO mice, ECs
388 derived from these animals remarkably demonstrated improved metabolic
389 characteristics (Figs. 3, 6). This complex metabolic phenotype observed in M4K4
390 iECKO mice after HFD may be explained by examining the blood and lymphatic
391 vascular systems as independent systems: though loss of Map4k4 is detrimental to the
392 lymphatic vascular system, it could be beneficial to the blood vascular system. Recent
393 studies have demonstrated that glycolysis and fatty acid oxidation are critical for blood
394 vessel angiogenesis and EC proliferation (10, 33), and we demonstrate here that
395 primary ECs lacking Map4k4 are resistant to senescence in culture and display
396 enhanced glycolytic and mitochondrial respiration (Fig. 6). The increase in endothelial
397 metabolism and reduced senescent phenotype is consistent with previously published
398 observations describing enhanced proliferation in ECs lacking Map4k4 (27). These
399 observations could partially explain why mice lacking endothelial Map4k4 were resistant
400 to capillary rarefaction in obesity (Fig. 5), which likely contributes to the improvement
401 observed in insulin sensitivity in HFD-fed M4K4 iECKO mice (Fig. 1). These data more
402 broadly suggest that the improved metabolic phenotype in M4K4 iECKO mice may be
403 due to ameliorating the detrimental effects of obesity on the blood vasculature. One
404 limitation to the interpretation of these metabolic data from isolated MLECs is that these
405 cultures represent a mixed population of lymphatic and blood ECs as they were isolated
406 using the pan-endothelial cell marker CD31. Future studies will separate out
407 phenotypes within the lymphatic and blood EC populations to address mechanistically
408 how Map4k4 regulates EC specification and function.

409 Chyle leakage can reportedly cause obesity; however, M4K4 iECKO mice
410 displayed similar weights as their Flox/Flox littermates (17, 31). Although not all M4K4
411 iECKO mice displayed visible chyle leakage after HFD, it is likely that all displayed
412 some degree of lymphatic dysfunction, as pathophysiological changes in lymphatic
413 vascular integrity can occur even if chyle leakage is not visible (17, 32). Furthermore,
414 despite chyle leakage, HFD-fed M4K4 iECKO mice demonstrated improved insulin
415 sensitivity (Fig. 1). One might expect that in the setting of dysfunctional lymphatic
416 vessels that lipid absorption from the intestine may be compromised in M4K4 iECKO
417 mice, which could contribute to the improved metabolic function in these animals.
418 Though excreted lipids were not examined, no alteration in plasma triglyceride or NEFA
419 content was observed between M4K4 iECKO mice and control littermates (Table 1);
420 furthermore, no change in weight or adiposity was observed. Future studies will be
421 conducted using Prox-1 ERT2 cre mice to delete Map4k4 in the lymphatic endothelium,
422 although these animals do have some cre expression in non-lymphatic tissues. (2).
423 Alternatively, Cx40-CreERT2 animals could be used to delete Map4k4 in arterial
424 endothelium only (3); these animal models will be critical to understand the contribution
425 of the blood vs. lymphatic endothelium to the metabolic phenotype that was observed
426 here.

427 In conclusion, we have demonstrated a complex role for protein kinase Map4k4
428 in developed vasculature to mediate the responses to high fat diet and thus regulate
429 glucose homeostasis in adult animals. Furthermore, these data suggest that Map4k4 is
430 not only required for vascular development, but also plays a significant role in vascular
431 inflammation and remodeling in pathology in adulthood. As the complexities of signaling

432 cascades are beginning to be understood in the blood vs. lymphatic vascular
433 endothelium, future studies assessing the contribution of these metabolic signaling
434 pathways in blood vs. lymphatic vascular compartments will provide great insight into
435 the mechanisms by which the vasculature contributes to glucose homeostasis and
436 insulin signaling in T2D.

437

438 **Acknowledgements**

439 The authors thank Joseph Virbasius, Silvia Corvera, and John Keaney for helpful
440 discussions and Joseph Virbasius for critical reading of the manuscript. We additionally
441 thank the UMASS Morphology core, Sarah Nicoloro, Phillip Yates and Chunyan Su for
442 assistance. This work was supported by NIH grant DK030898 to M.P.C. Current
443 addresses: ¹Pfizer, Inc., Cambridge, MA USA, ²Laboratory for Molecular Medicine,
444 Partners Health Care, Cambridge, MA, USA, ³Koch Institute for Integrative Cancer
445 Research, Massachusetts Institute of Technology, Cambridge, MA USA, ⁴Stemcell
446 Technologies, Inc., Cambridge, MA USA, ⁵Cardiovascular Division, Department of
447 Medicine, University of Massachusetts Medical School, 55 Lake Avenue North,
448 Worcester, MA, USA.

449

450 **References**

- 451 1. **Alitalo K.** The lymphatic vasculature in disease. *Nat Med* 17: 1371-1380, 2011.
452 2. **Bazigou E, Lyons OT, Smith A, Venn GE, Cope C, Brown NA, and Mäkinen T.**
453 Genes regulating lymphangiogenesis control venous valve formation and maintenance in
454 mice. *J Clin Invest* 121: 2984-2992, 2011.
455 3. **Beyer S, Kelly RG, and Miquerol L.** Inducible Cx40-Cre expression in the cardiac
456 conduction system and arterial endothelial cells. *Genesis* 49: 83-91, 2011.

- 457 4. **Bonner JS, Lantier L, Hasenour CM, James FD, Bracy DP, and Wasserman DH.**
 458 Muscle-specific vascular endothelial growth factor deletion induces muscle capillary
 459 rarefaction creating muscle insulin resistance. *Diabetes* 62: 572-580, 2013.
- 460 5. **Brakenhielm E, Cao R, Gao B, Angelin B, Cannon B, Parini P, and Cao Y.**
 461 Angiogenesis inhibitor, TNP-470, prevents diet-induced and genetic obesity in mice. *Circ*
 462 *Res* 94: 1579-1588, 2004.
- 463 6. **Cao Y.** Adipose tissue angiogenesis as a therapeutic target for obesity and metabolic
 464 diseases. *Nat Rev Drug Discov* 9: 107-115, 2010.
- 465 7. **Card CM, Yu SS, and Swartz MA.** Emerging roles of lymphatic endothelium in
 466 regulating adaptive immunity. *J Clin Invest* 124: 943-952, 2014.
- 467 8. **Danai LV, Flach RJ, Virbasius JV, Menendez LG, Jung DY, Kim JH, Kim JK, and**
 468 **Czech MP.** Inducible Deletion of Protein Kinase Map4k4 in Obese Mice Improves Insulin
 469 Sensitivity in Liver and Adipose Tissues. *Mol Cell Biol* 35: 2356-2365, 2015.
- 470 9. **Deiuliis J, Shah Z, Shah N, Needleman B, Mikami D, Narula V, Perry K, Hazey J,**
 471 **Kampfrath T, Kollengode M, Sun Q, Satoskar AR, Lumeng C, Moffatt-Bruce S, and**
 472 **Rajagopalan S.** Visceral adipose inflammation in obesity is associated with critical
 473 alterations in regulatory cell numbers. *PloS one* 6: e16376, 2011.
- 474 10. **Eelen G, de Zeeuw P, Simons M, and Carmeliet P.** Endothelial cell metabolism in
 475 normal and diseased vasculature. *Circ Res* 116: 1231-1244, 2015.
- 476 11. **Erusalimsky JD.** Vascular endothelial senescence: from mechanisms to
 477 pathophysiology. *J Appl Physiol (1985)* 106: 326-332, 2009.
- 478 12. **Feuerer M, Herrero L, Cipolletta D, Naaz A, Wong J, Nayer A, Lee J, Goldfine AB,**
 479 **Benoist C, Shoelson S, and Mathis D.** Lean, but not obese, fat is enriched for a unique
 480 population of regulatory T cells that affect metabolic parameters. *Nat Med* 15: 930-939,
 481 2009.
- 482 13. **Frisbee JC, Goodwill AG, Frisbee SJ, Butcher JT, Brock RW, Olfert IM,**
 483 **DeVallance ER, and Chantler PD.** Distinct temporal phases of microvascular rarefaction in
 484 skeletal muscle of obese Zucker rats. *American journal of physiology Heart and circulatory*
 485 *physiology* 307: H1714-1728, 2014.
- 486 14. **Gealekman O, Burkart A, Chouinard M, Nicoloso SM, Straubhaar J, and Corvera**
 487 **S.** Enhanced angiogenesis in obesity and in response to PPARgamma activators through
 488 adipocyte VEGF and ANGPTL4 production. *Am J Physiol Endocrinol Metab* 295: E1056-1064,
 489 2008.
- 490 15. **Gealekman O, Guseva N, Hartigan C, Apotheker S, Gorgoglione M, Gurav K,**
 491 **Tran KV, Straubhaar J, Nicoloso S, Czech MP, Thompson M, Perugini RA, and Corvera**
 492 **S.** Depot-specific differences and insufficient subcutaneous adipose tissue angiogenesis in
 493 human obesity. *Circulation* 123: 186-194, 2011.
- 494 16. **Guilherme A, Virbasius JV, Puri V, and Czech MP.** Adipocyte dysfunctions linking
 495 obesity to insulin resistance and type 2 diabetes. *Nat Rev Mol Cell Biol* 9: 367-377, 2008.
- 496 17. **Harvey NL, Srinivasan RS, Dillard ME, Johnson NC, Witte MH, Boyd K, Sleeman**
 497 **MW, and Oliver G.** Lymphatic vascular defects promoted by Prox1 haploinsufficiency
 498 cause adult-onset obesity. *Nature genetics* 37: 1072-1081, 2005.
- 499 18. **Kubota T, Kubota N, and Kadowaki T.** The role of endothelial insulin signaling in
 500 the regulation of glucose metabolism. *Reviews in endocrine & metabolic disorders* 14: 207-
 501 216, 2013.

- 502 19. **Kubota T, Kubota N, Kumagai H, Yamaguchi S, Kozono H, Takahashi T, Inoue M,**
503 **Itoh S, Takamoto I, Sasako T, Kumagai K, Kawai T, Hashimoto S, Kobayashi T, Sato M,**
504 **Tokuyama K, Nishimura S, Tsunoda M, Ide T, Murakami K, Yamazaki T, Ezaki O,**
505 **Kawamura K, Masuda H, Moroi M, Sugi K, Oike Y, Shimokawa H, Yanagihara N,**
506 **Tsutsui M, Terauchi Y, Tobe K, Nagai R, Kamata K, Inoue K, Kodama T, Ueki K, and**
507 **Kadowaki T.** Impaired insulin signaling in endothelial cells reduces insulin-induced
508 glucose uptake by skeletal muscle. *Cell metabolism* 13: 294-307, 2011.
- 509 20. **Lim HY, Rutkowski JM, Helft J, Reddy ST, Swartz MA, Randolph GJ, and Angeli V.**
510 Hypercholesterolemic mice exhibit lymphatic vessel dysfunction and degeneration. *The*
511 *American journal of pathology* 175: 1328-1337, 2009.
- 512 21. **Lim HY, Thiam CH, Yeo KP, Bisioendial R, Hii CS, McGrath KC, Tan KW, Heather**
513 **A, Alexander JS, and Angeli V.** Lymphatic vessels are essential for the removal of
514 cholesterol from peripheral tissues by SR-BI-mediated transport of HDL. *Cell metabolism*
515 17: 671-684, 2013.
- 516 22. **Nishimura S, Manabe I, Nagasaki M, Seo K, Yamashita H, Hosoya Y, Ohsugi M,**
517 **Tobe K, Kadowaki T, Nagai R, and Sugiura S.** In vivo imaging in mice reveals local cell
518 dynamics and inflammation in obese adipose tissue. *J Clin Invest* 118: 710-721, 2008.
- 519 23. **Oh DY, Morinaga H, Talukdar S, Bae EJ, and Olefsky JM.** Increased macrophage
520 migration into adipose tissue in obese mice. *Diabetes* 61: 346-354, 2012.
- 521 24. **Pannekoek WJ, Linnemann JR, Brouwer PM, Bos JL, and Rehmann H.** Rap1 and
522 Rap2 antagonistically control endothelial barrier resistance. *PLoS one* 8: e57903, 2013.
- 523 25. **Randolph GJ, and Miller NE.** Lymphatic transport of high-density lipoproteins and
524 chylomicrons. *J Clin Invest* 124: 929-935, 2014.
- 525 26. **Roth Flach RJ, Danai LV, DiStefano MT, Kelly M, Menendez LG, Jurczyk A,**
526 **Sharma RB, Jung DY, Kim JH, Kim JK, Bortell R, Alonso LC, and Czech MP.** Protein
527 Kinase Mitogen-activated Protein Kinase Kinase Kinase Kinase 4 (MAP4K4) Promotes
528 Obesity-induced Hyperinsulinemia. *J Biol Chem* 291: 16221-16230, 2016.
- 529 27. **Roth Flach RJ, Guo CA, Danai LV, Yawe JC, Gujja S, Edwards YJ, and Czech MP.**
530 Endothelial Mitogen-Activated Protein Kinase Kinase Kinase Kinase 4 Is Critical for
531 Lymphatic Vascular Development and Function. *Mol Cell Biol* 36: 1740-1749, 2016.
- 532 28. **Roth Flach RJ, Skoura A, Matevossian A, Danai LV, Zheng W, Cortes C,**
533 **Bhattacharya SK, Aouadi M, Hagan N, Yawe JC, Vangala P, Menendez LG, Cooper MP,**
534 **Fitzgibbons TP, Buckbinder L, and Czech MP.** Endothelial protein kinase MAP4K4
535 promotes vascular inflammation and atherosclerosis. *Nature communications* 6: 8995,
536 2015.
- 537 29. **Russo HM, Wickenheiser KJ, Luo W, Ohman MK, Franchi L, Wright AP, Bodary**
538 **PF, Nunez G, and Eitzman DT.** P-selectin glycoprotein ligand-1 regulates adhesive
539 properties of the endothelium and leukocyte trafficking into adipose tissue. *Circ Res* 107:
540 388-397, 2010.
- 541 30. **Sato C, Shikata K, Hirota D, Sasaki M, Nishishita S, Miyamoto S, Koderu R,**
542 **Ogawa D, Tone A, Kataoka HU, Wada J, Kajitani N, and Makino H.** P-selectin
543 glycoprotein ligand-1 deficiency is protective against obesity-related insulin resistance.
544 *Diabetes* 60: 189-199, 2011.
- 545 31. **Sawane M, Kajiya K, Kidoya H, Takagi M, Muramatsu F, and Takakura N.** Apelin
546 inhibits diet-induced obesity by enhancing lymphatic and blood vessel integrity. *Diabetes*
547 62: 1970-1980, 2013.

- 548 32. **Scallan JP, Hill MA, and Davis MJ.** Lymphatic vascular integrity is disrupted in type
549 2 diabetes due to impaired nitric oxide signalling. *Cardiovascular research* 107: 89-97,
550 2015.
- 551 33. **Schoors S, Bruning U, Missiaen R, Queiroz KC, Borgers G, Elia I, Zecchin A,**
552 **Cantelmo AR, Christen S, Goveia J, Heggermont W, Godde L, Vinckier S, Van**
553 **Veldhoven PP, Eelen G, Schoonjans L, Gerhardt H, Dewerchin M, Baes M, De Bock K,**
554 **Ghesquiere B, Lunt SY, Fendt SM, and Carmeliet P.** Fatty acid carbon is essential for
555 dNTP synthesis in endothelial cells. *Nature* 520: 192-197, 2015.
- 556 34. **Shimizu I, Aprahamian T, Kikuchi R, Shimizu A, Papanicolaou KN,**
557 **MacLauchlan S, Maruyama S, and Walsh K.** Vascular rarefaction mediates whitening of
558 brown fat in obesity. *J Clin Invest* 124: 2099-2112, 2014.
- 559 35. **Shoelson SE, Lee J, and Goldfine AB.** Inflammation and insulin resistance. *J Clin*
560 *Invest* 116: 1793-1801, 2006.
- 561 36. **Simons M, Alitalo K, Annex BH, Augustin HG, Beam C, Berk BC, Byzova T,**
562 **Carmeliet P, Chilian W, Cooke JP, Davis GE, Eichmann A, Iruela-Arispe ML, Keshet E,**
563 **Sinusas AJ, Ruhrberg C, Woo YJ, Dimmeler S, American Heart Association Council on**
564 **Basic Cardiovascular S, Council on Cardiovascular S, and Anesthesia.** State-of-the-Art
565 Methods for Evaluation of Angiogenesis and Tissue Vascularization: A Scientific Statement
566 From the American Heart Association. *Circ Res* 116: e99-e132, 2015.
- 567 37. **Sun K, Wernstedt Asterholm I, Kusminski CM, Bueno AC, Wang ZV, Pollard JW,**
568 **Brekken RA, and Scherer PE.** Dichotomous effects of VEGF-A on adipose tissue
569 dysfunction. *Proc Natl Acad Sci U S A* 109: 5874-5879, 2012.
- 570 38. **Sung HK, Doh KO, Son JE, Park JG, Bae Y, Choi S, Nelson SM, Cowling R, Nagy K,**
571 **Michael IP, Koh GY, Adamson SL, Pawson T, and Nagy A.** Adipose vascular endothelial
572 growth factor regulates metabolic homeostasis through angiogenesis. *Cell metabolism* 17:
573 61-72, 2013.
- 574 39. **Taher M, Nakao S, Zandi S, Melhorn MI, Hayes KC, and Hafezi-Moghadam A.**
575 Phenotypic transformation of intimal and adventitial lymphatics in atherosclerosis: a
576 regulatory role for soluble VEGF receptor 2. *FASEB journal : official publication of the*
577 *Federation of American Societies for Experimental Biology* 30: 2490-2499, 2016.
- 578 40. **Tang X, Guilherme A, Chakladar A, Powelka AM, Konda S, Virbasius JV,**
579 **Nicoloro SM, Straubhaar J, and Czech MP.** An RNA interference-based screen identifies
580 MAP4K4/NIK as a negative regulator of PPARgamma, adipogenesis, and insulin-responsive
581 hexose transport. *Proc Natl Acad Sci U S A* 103: 2087-2092, 2006.
- 582 41. **Vicent D, Ilany J, Kondo T, Naruse K, Fisher SJ, Kisanuki YY, Bursell S,**
583 **Yanagisawa M, King GL, and Kahn CR.** The role of endothelial insulin signaling in the
584 regulation of vascular tone and insulin resistance. *J Clin Invest* 111: 1373-1380, 2003.
- 585 42. **Villaret A, Galitzky J, Decaunes P, Esteve D, Marques MA, Sengenès C, Chiotasso**
586 **P, Tchkonja T, Lafontan M, Kirkland JL, and Bouloumie A.** Adipose tissue endothelial
587 cells from obese human subjects: differences among depots in angiogenic, metabolic, and
588 inflammatory gene expression and cellular senescence. *Diabetes* 59: 2755-2763, 2010.
- 589 43. **Virbasius JV, and Czech MP.** Map4k4 Signaling Nodes in Metabolic and
590 Cardiovascular Diseases. *Trends Endocrinol Metab* 27: 484-492, 2016.
- 591 44. **Wang Y, Nakayama M, Pitulescu ME, Schmidt TS, Bochenek ML, Sakakibara A,**
592 **Adams S, Davy A, Deutsch U, Luthi U, Barberis A, Benjamin LE, Makinen T, Nobes CD,**

- 593 **and Adams RH.** Ephrin-B2 controls VEGF-induced angiogenesis and lymphangiogenesis.
594 *Nature* 465: 483-486, 2010.
- 595 45. **Weisberg SP, McCann D, Desai M, Rosenbaum M, Leibel RL, and Ferrante AW,**
596 **Jr.** Obesity is associated with macrophage accumulation in adipose tissue. *J Clin Invest* 112:
597 1796-1808, 2003.
- 598 46. **Wellen KE, and Hotamisligil GS.** Inflammation, stress, and diabetes. *J Clin Invest*
599 115: 1111-1119, 2005.
- 600 47. **Wilson PW, D'Agostino RB, Parise H, Sullivan L, and Meigs JB.** Metabolic
601 syndrome as a precursor of cardiovascular disease and type 2 diabetes mellitus. *Circulation*
602 112: 3066-3072, 2005.
- 603 48. **Xu H, Barnes GT, Yang Q, Tan G, Yang D, Chou CJ, Sole J, Nichols A, Ross JS,**
604 **Tartaglia LA, and Chen H.** Chronic inflammation in fat plays a crucial role in the
605 development of obesity-related insulin resistance. *J Clin Invest* 112: 1821-1830, 2003.
- 606 49. **Yokoyama M, Okada S, Nakagomi A, Moriya J, Shimizu I, Nojima A, Yoshida Y,**
607 **Ichimiya H, Kamimura N, Kobayashi Y, Ohta S, Fruttiger M, Lozano G, and Minamino**
608 **T.** Inhibition of endothelial p53 improves metabolic abnormalities related to dietary
609 obesity. *Cell Rep* 7: 1691-1703, 2014.
- 610
- 611
- 612 **Conflict of Interest:** The authors declare no financial conflicts of interest.

613 **Figure Legends**

614

615 **Figure 1. Improved glucose tolerance in the context of no change in body**
616 **weight in HFD-fed M4K4 iECKO mice. A.** Tamoxifen injection and deletion
617 scheme of endothelial Map4k4. **B-F.** Mice were fed chow or HFD for 16 weeks
618 starting 2 weeks post-tamoxifen injections. **B.** Weight curves of chow and HFD-
619 fed Flox/Flox and M4K4 iECKO mice (N=9-11). **C-F.** Tissue weights of HFD-fed
620 Flox/Flox and M4K4 iECKO mice. **C.** SAT, **D.** eWAT, **E.** Liver, **F.** Spleen (N=9-
621 11). **G.** Blood glucose levels during a glucose tolerance test. **H.** Percent glucose
622 remaining during an insulin tolerance test. (ANOVA *; $p < 0.05$, N=8-9 chow, 13-15
623 HFD).

624

625 **Figure 2. Reduced expression of genes encoding proteins in inflammation**
626 **pathways in HFD-fed M4K4 iECKO livers.** Flox/Flox or M4K4 iECKO mice
627 were fed HFD for 16 weeks starting 2 weeks post-tamoxifen injections. **A.**
628 Representative H&E stained histological liver sections of at least 5 mice per
629 genotype. Scale bars represent 100 μ m. **B-C.** Whole liver was isolated, and
630 quantitative rtPCR was performed. **B.** leukocyte adhesion molecules, **C.**
631 leukocyte markers (*; $p < 0.05$, N=8-9).

632

633 **Figure 3. Chyle leakage and eWAT inflammation in HFD-fed M4K4 iECKO**
634 **mice.** Flox/Flox or M4K4 iECKO mice were fed chow or HFD for 16 weeks
635 starting 2 weeks post-tamoxifen injections. **A.** Representative image of HFD-fed

636 M4K4 iECKO mouse displaying chyle in the abdominal cavity. **B.** H&E staining of
637 eWAT from Flox/Flox or M4K4 iECKO mice after chow or HFD. **C.** H&E staining
638 of SAT, rWAT, mWAT and intrascapular BAT from Flox/Flox or M4K4 iECKO
639 mice. Scale bar represents 100 μ m. Images are representative of at least 5
640 animals per genotype.

641

642 **Figure 4. Lymphocyte accumulation in adipose tissue of HFD-fed M4K4**

643 **iECKO mice. A-F.** Flox/Flox or M4K4 iECKO mice were fed chow or HFD for 16
644 weeks starting 2 weeks post-tamoxifen injections. Flow cytometry was performed
645 from HFD-fed Flox/Flox or M4K4 iECKO mouse SVF. **A-B.** Representative flow
646 cytometry panels. **A.** Cd11b and F4/80-positive macrophages. **B.** Cd3+ and Cd4
647 or Cd8 positive lymphocytes. **C.** Quantitation of flow cytometry for Cd11b and
648 F4/80-positive macrophages or Cd11b, F4/80 and Cd11c-positive macrophages
649 as a percentage of cells in SVF (N=8-12). **D.** qRT-PCR for macrophage marker
650 genes and macrophage-derived cytokines from whole adipose tissue as
651 normalized to *36b4* (N=8-11). **E.** Quantitation of flow cytometry for Cd3, Cd4-,
652 Cd8-, Treg (foxp3+/Cd25+) and Cd19- positive lymphocytes as a percentage of
653 cells in SVF (*; p<0.05, **; p<0.005, N=3-6, 7-11). **F.** qRT-PCR for lymphocyte
654 marker genes and lymphocyte-derived cytokines from whole adipose tissue as
655 normalized to *36b4* (*; p<0.05, N=8-11).

656

657 **Figure 5. Protection from capillary rarefaction in skeletal muscle of M4K4**

658 **iECKO mice.** Mice were fed chow (**A -F, I-J**) or HFD (**G-H, I-J**) for 16 weeks

659 starting 2 weeks post-tamoxifen injections. **A-D.** Chow-fed mice were injected i.v.
660 with Evans blue dye for one hour, dye was perfused out with PBS, extracted from
661 tissues overnight, and assessed spectrophotometrically (N=5-9). **E-J** Tissues
662 were stained with isolectin B4 as a measure of vascular density. **E-F.** Aortas
663 were isolated, embedded in collagen, and treated with Vegf-A. **E.** Representative
664 images. Scale bar represents 250 μ m. **F.** Quantification of the average number of
665 iB4-positive sprouts after 6 days (N=10-11, average of 7-16 technical replicates
666 per animal). **G-H.** eWAT was isolated and stained with iB4. **G.** Representative
667 images of HFD-fed Flox/Flox and M4K4 iECKO eWAT. Scale bar represents 100
668 μ m. **H.** Quantitation of iB4-stained area (N=8-9). **I-J.** Soleus muscle was isolated
669 and stained with iB4. **I.** Representative images of chow-fed (upper) and HFD-fed
670 (lower) Flox/Flox and M4K4 iECKO soleus muscle. Scale bars represent 100 μ m.
671 **J.** Quantitation of iB4-stained area (*; $p < 0.05$, N=5-8).

672

673 **Figure 6. Reduced senescence and enhanced metabolism in ECs lacking**
674 **Map4k4. A-F.** Primary MLECs were derived from chow-fed Flox/Flox or M4K4
675 iECKO mice. **A-B.** Confluent MLECs were stained for endogenous β -
676 galactosidase activity and normalized to nuclei number as measured by Hoechst
677 staining. **A.** Representative image; scale bar represents 100 μ m. **B.** Quantitation
678 of stained area (**; $p < 0.005$, N=9-10). **C.** Oxygen consumption rate profile of
679 MLEC mitochondrial respiration. Vertical lines indicate the time of addition of
680 oligomycin, FCCP, or antimycin A and rotenone. **D.** Quantitation of mitochondrial
681 respiration; values are normalized to protein content (*; $p < 0.05$, N=5). **E.**

682 Extracellular acidification rate profile demonstrating glycolytic function in MLECs.
 683 Vertical lines indicate the time of glucose, oligomycin, and 2-DG addition. **F.**
 684 Quantitation of glycolytic function; values are normalized to protein content (*;
 685 $p < 0.05$, $N = 7$).

686

687

688 **Table 1. RT-PCR primer sequences.**

Gene	Forward	Reverse
F4/80	CCCCAGTGTCTTACAGAGTG	GTGCCCAGAGTGGATGTCT
Cd68	CCATCCTTCACGATGACACCT	GGCAGGGTTATGAGTGACAGTT
Ccl-2	TTAAAAACCTGGATCGGAACCAA	GCATTAGCTTCAGATTTACGGGT
36b4	TCCAGGCTTTGGGCATCA	CTTTATCAGCTGCACATCACTCAGA
Ilgam	ATGGACGCTGATGGCAATACC	TCCCCATTACAGTCTCCCA
Ilgax	CTGGATAGCCTTTCTTCTGCTG	GCACACTGTGTCCGAACCTCA
Il-1b	GCAACTGTTCTGAACTCAACT	ATCTTTTGGGGTCCGTCAACT
Il-6	TAGTCTTCTACCCCAATTTCC	TTGGTCCTTAGCCACTCCTTC
Cd3	AGTGCAGTTCGGGAACAGAAG	GATTGGCTACTCTGCTGGGT
Cd4	TCACCTGGAAGTTCTCTGACC	GGAATCAAACGATCAAACCTGCG
Cd8	CCGTTGACCCGCTTTCTGT	CGGCGTCCATTTTCTTTGGAA
Foxp3	GGTACACCCAGGAAAGACAGC	AAGACCTTCTCACAACCAGGC
Il-4	GGTCTCAACCCCCAGCTAGT	GCCGATGATCTCTCTCAAGTGAT
Il-10	GCTCTTACTGACTGGCATGAG	CGCAGCTCTAGGAGCATGTG
Ifng	ATGAACGCTACACACTGCATC	CCATCCTTTTGCCAGTTCCCTC
Il-13	CCTGGCTCTTGCTTGCCTT	GGTCTTGTGTGATGTTGCTCA
Il-17	TCAGCGTGTCCAAACACTGAG	CGCCAAGGGAGTTAAAGACTT
Il-21	GGACCCTTGTCTGTCTGGTAG	TGTGGAGCTGATAGAAGTTCAGG
Pepck	CTGCATAACGGTCTGGACTTC	CAGCAACTGCCCGTACTCC
G6pc	CGACTCGCTATCTCCAAGTGA	GTTGAACCAGTCTCCGACCA
Gck	TGAGCCGGATGCAGAAGGA	GCAACATCTTACACTGGCCT
Fasn	GGAGGTGGTGATAGCCGCTAT	TGGGTAATCCATAGAGCCCAG
Cidec	ATCAGAACAGCGCAAGAAGA	CAGCTTGTACAGGTCTGAAGG
Cidea	TGACATTCATGGGATTGCAGAC	GGCCAGTTGTGATGACTAAGAC
Cd14	CTCTGTCCTTAAAGCGGCTTAC	GTTGCGGAGGTTCAAGATGTT
Ccl-3	TTCTCTGTACCATGACACTCTGC	CGTGGAAATCTTCCGGCTGTAG
Ccl-5	TCGAGTGACAAACACGACTGC	GCTGCTTTGCCTACCTCTCC
Tnf-a	CAGGCGGTGCCTATGTCTC	CGATCACCCCGAAGTTCAGTAG
Icam-1	GTGATGCTCAGGTATCCATCCA	CACAGTTCTCAAAGCACAGCG
Vcam-1	AGTTGGGGATTTCGGTTGTTCT	CCCCTCATTCTTACCACCC

Sele	ATGAAGCCAGTGCATACTGTC	CGGTGAATGTTTCAGATTGGAGT
Selp	CATCTGGTTCAGTGCTTTGATCT	ACCCGTGAGTTATTCCATGAGT

689

690 **Table 2. Plasma analysis.**

	Flox/Flox	M4K4 iECKO
Insulin (ng/mL)	4.22 ± 0.63	2.93 ± 0.22 \$
NEFA (nmol/L)	0.37 ± 0.07	0.29 ± 0.07
Triglycerides	0.90 ± 0.09	1.26 ± 0.32

691

692 **Table 2.** Flox/Flox and M4K4 iECKO mice were fed HFD for 16 weeks. Animals
 693 were fasted overnight, and plasma insulin, non-esterified fatty acids (NEFA), and
 694 triglyceride levels were assessed (\$; p=0.06, N=3-8).

695

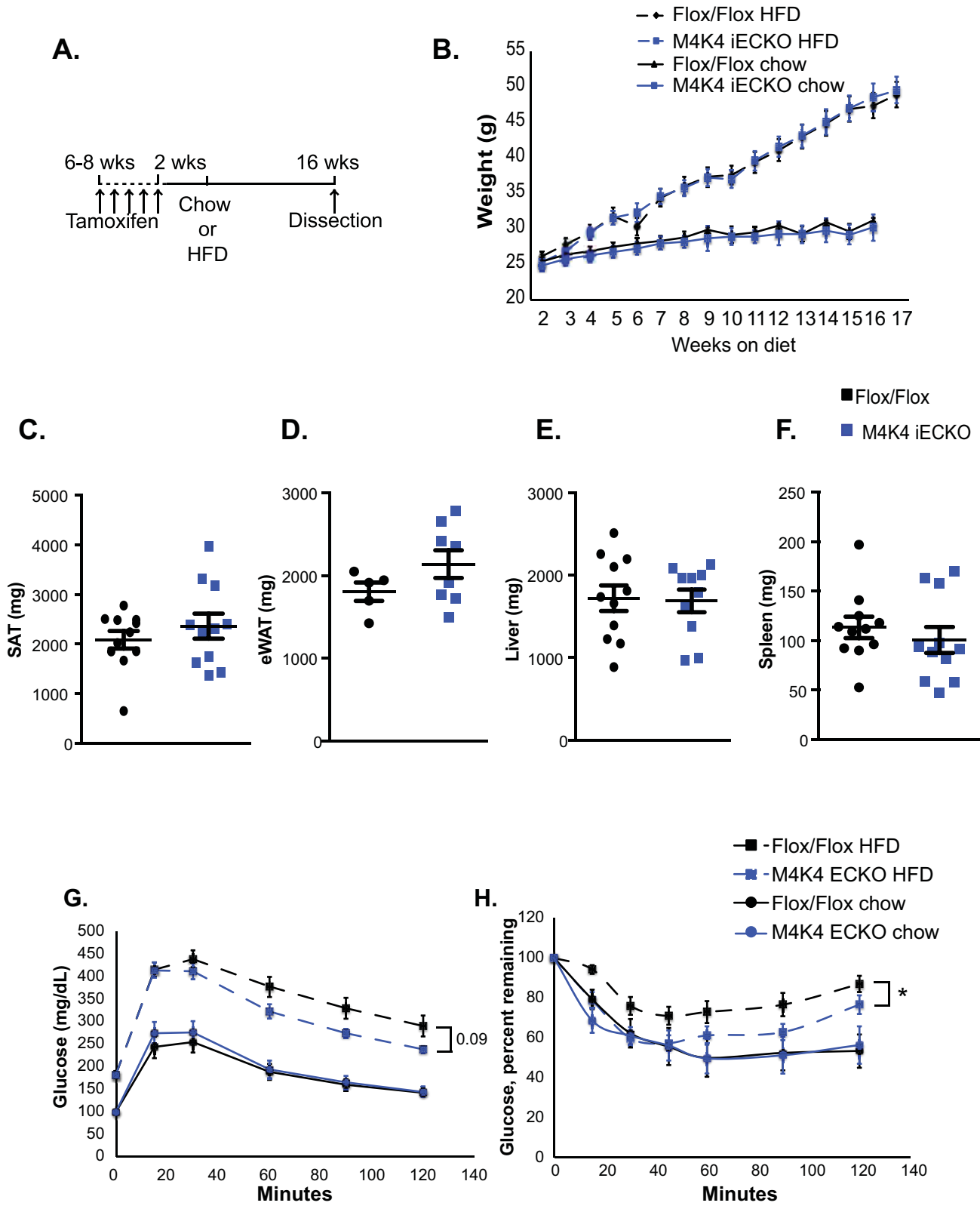


Figure 1

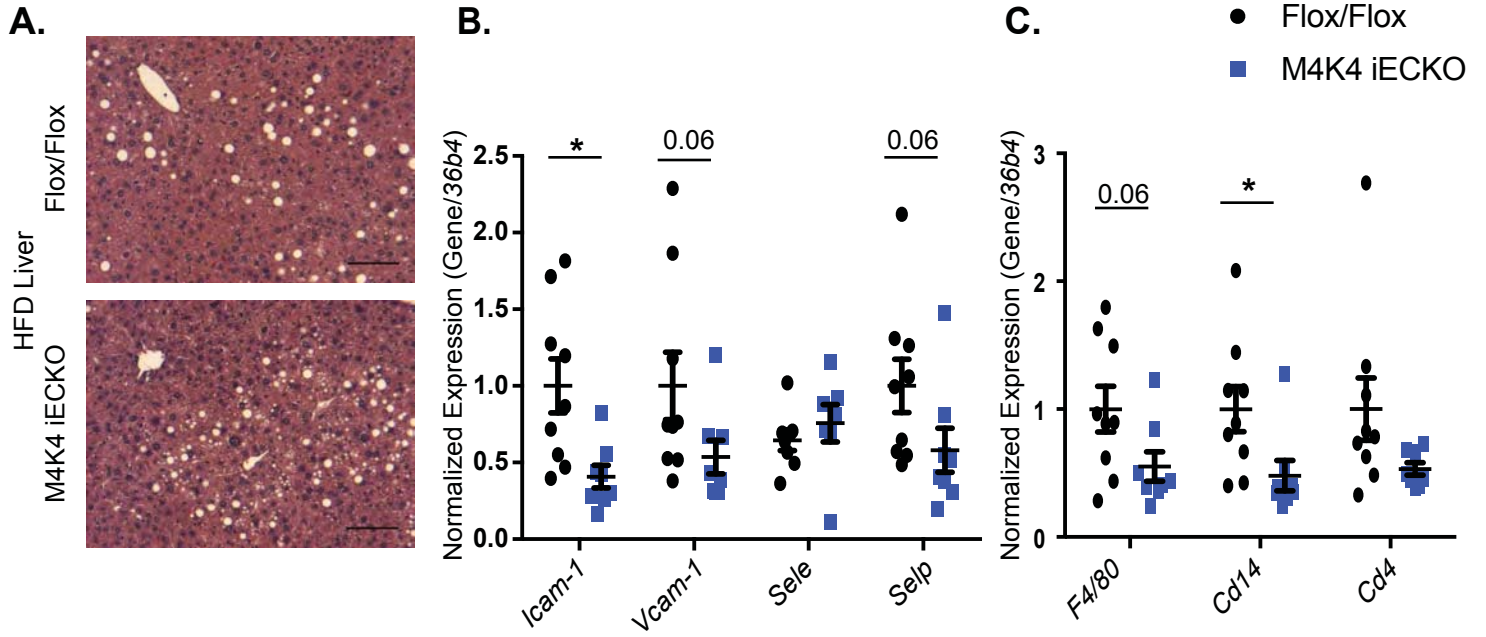
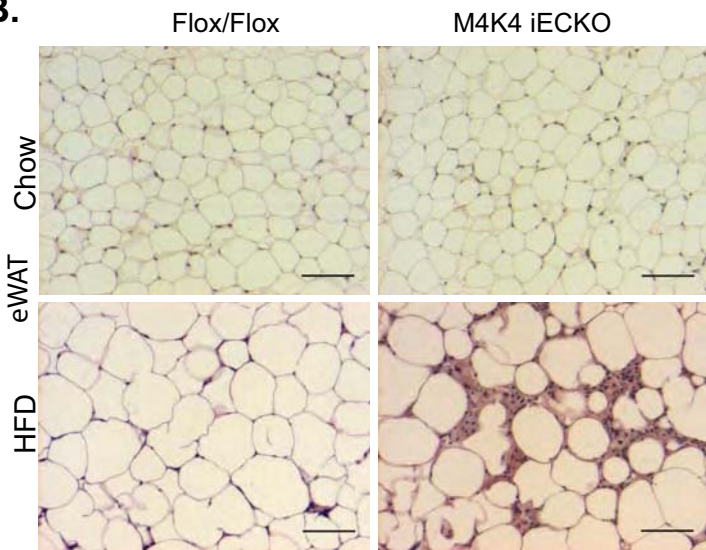


Figure 2

A.



B.



C.

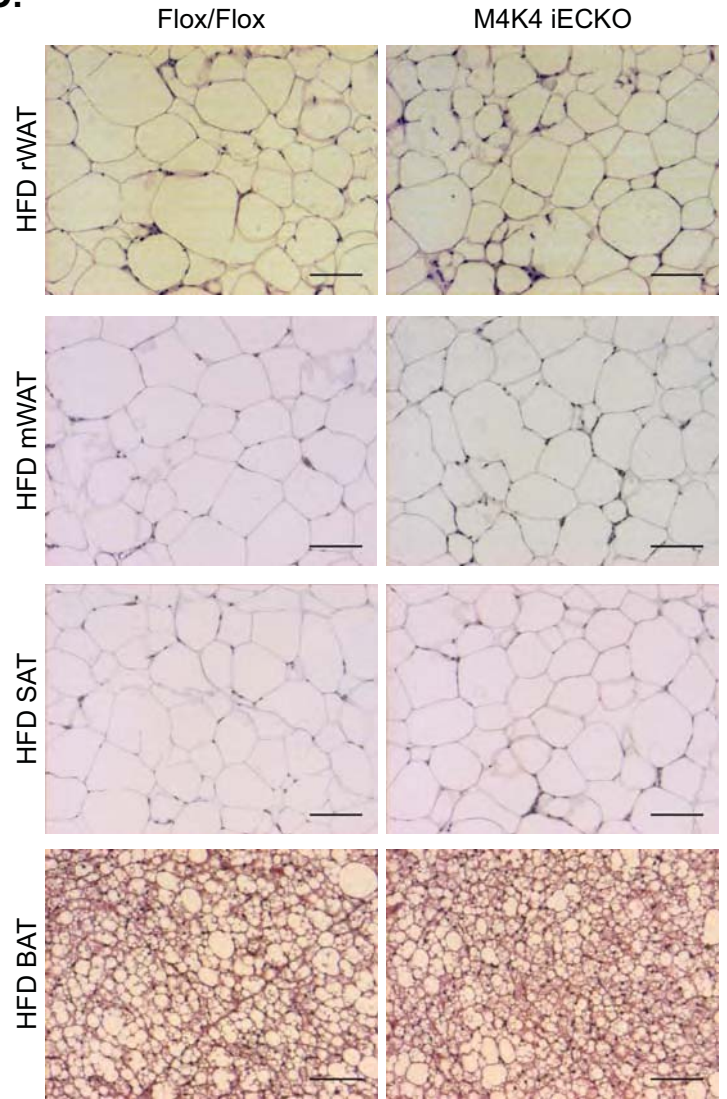
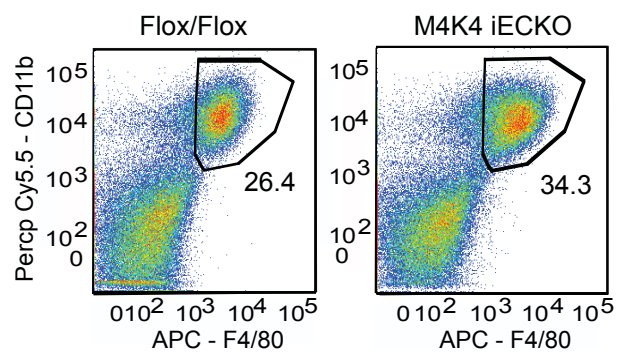
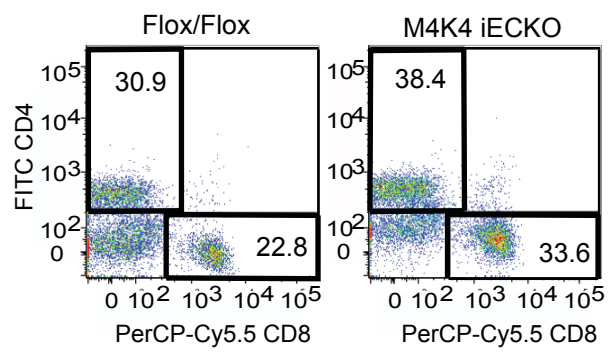
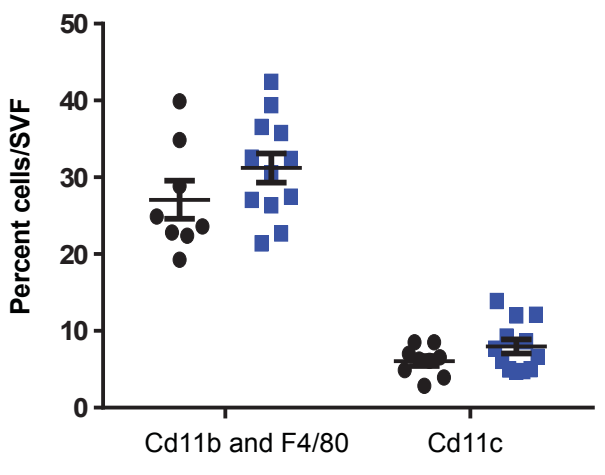
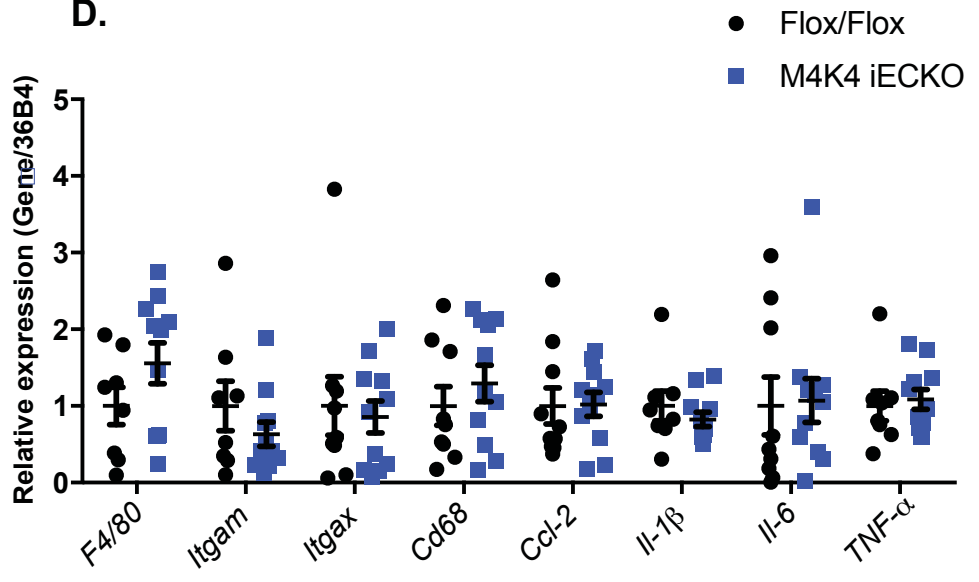
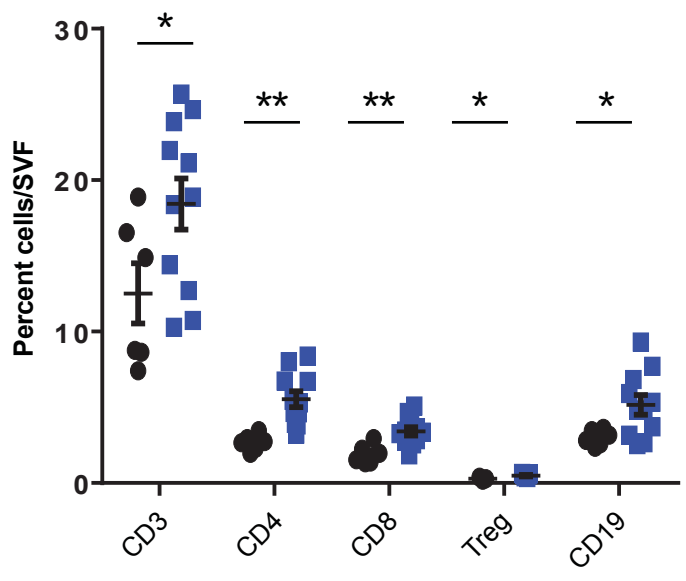
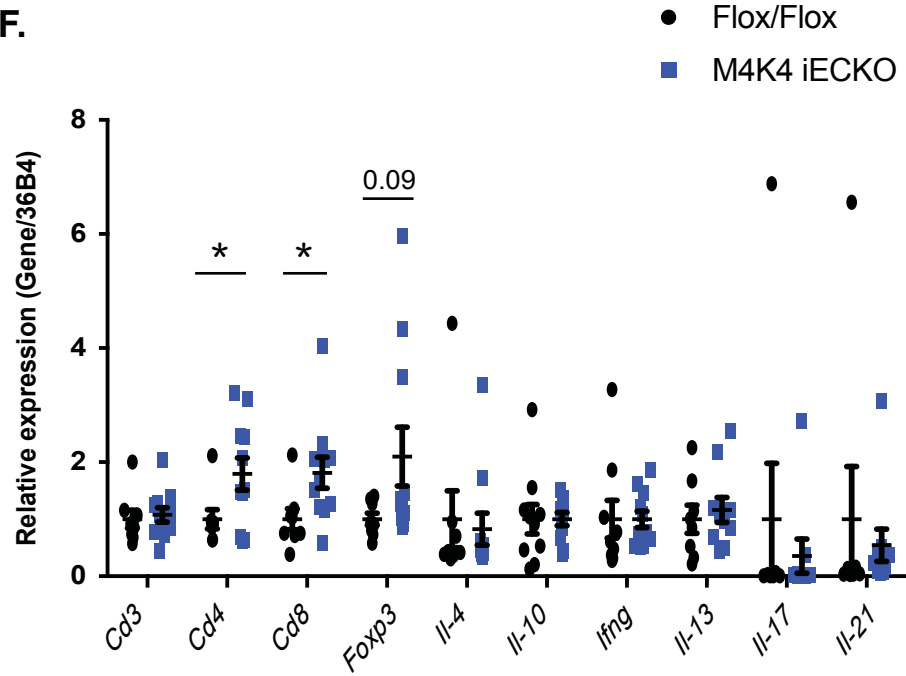


Figure 3

A.**B.****C.****D.****E.****F.****Figure 4**

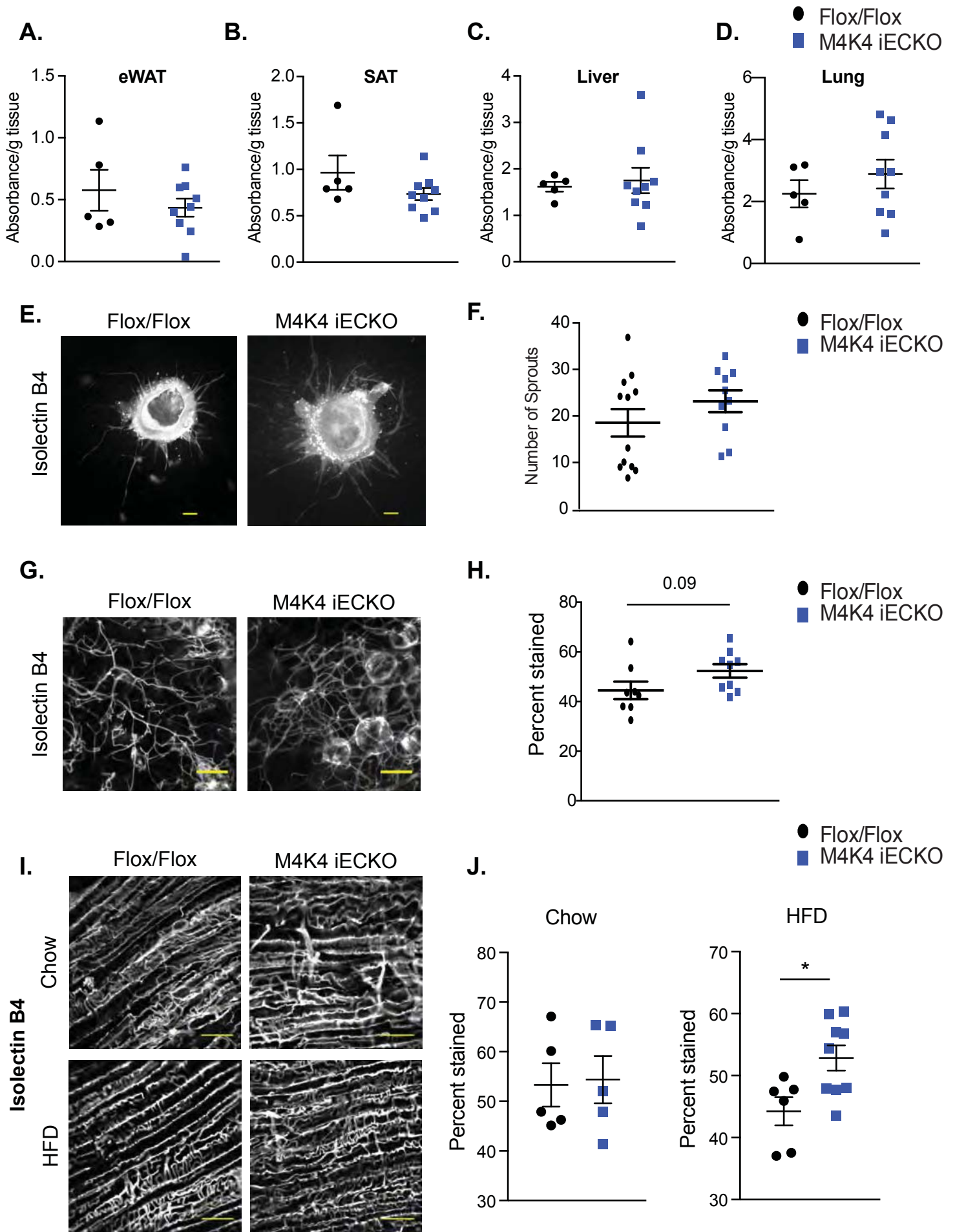


Figure 5

